HHS Public Access

Author manuscript

ACS Nano. Author manuscript; available in PMC 2022 July 10.

Published in final edited form as:

ACS Nano. 2022 February 22; 16(2): 2741–2755. doi:10.1021/acsnano.1c09688.

Scaffold-Free Spheroids with Two-Dimensional Hetero-Nano-Layers (2DHNL) Enabling Stem Cell and Osteogenic Factor Co-Delivery for Bone Repair

Xifeng Liu[†,‡], **Linli Li**[†,‡], **Bipin Gaihre**[†,‡], **Sungjo Park**[§], **Yong Li**[†,‡], **Andre Terzic**[§], **Benjamin D. Elder**[†,‡,‖], **Lichun Lu**[†,‡,*]

[†]Department of Physiology and Biomedical Engineering, Mayo Clinic, Rochester, MN 55905, USA.

[‡]Department of Orthopedic Surgery, Mayo Clinic, Rochester, MN 55905, USA.

[§]Department of Cardiovascular Diseases and Center for Regenerative Medicine, Mayo Clinic, Rochester, Minnesota 55905, USA.

[‖]Department of Neurologic Surgery, Mayo Clinic, Rochester, MN 55905, USA.

Abstract

Scaffold-free spheroids offer great potential as a direct supply of cells for bottom-up bone tissue engineering. However, the building of functional spheroids with both cells and bioactive signals remains challenging. Here, we engineered functional spheroids with mesenchymal stem cells (MSCs) and two-dimensional hetero-nano-layers (2DHNL) that consisted of black phosphorus (BP) and graphene oxide (GO) to create a 3D cell-instructive microenvironment for large defect bone repair. The effects of the engineered 2D materials on the proliferation, osteogenic differentiation of stem cells was evaluated in an *in vitro* 3D spheroidal microenvironment. Excellent *in vivo* support of osteogenesis of MSCs, neovascularization, and bone regeneration was achieved after transplanting these engineered spheroids into critical-sized rat calvarial defects. Further loading of osteogenic factor dexamethasone (DEX) on the 2DHNL showed outstanding *in vivo* osteogenic induction and bone regrowth without prior in vitro culture in osteogenic medium. The shortened overall culture time would be advantageous for clinical translation. These functional spheroids impregnated with engineered 2DHNL enabling stem cell and osteogenic factor co-delivery could be promising functional building blocks to provide cells and differential clues in an all-in-one system to create large tissues for time-effective *in vivo* bone repair.

Keywords

stem cells; spheroids; two-dimensional materials; bone regeneration; hetero-nano-layers (HNL)

[*]**Corresponding Author: Lichun Lu** - Department of Physiology and Biomedical Engineering, Mayo Clinic, Rochester, MN 55905, USA.; Department of Orthopedic Surgery, Mayo Clinic, Rochester, MN 55905, USA. Lu.Lichun@mayo.edu Tel.: 507-284-2267 Fax: 507-284-5075.

The authors declare no competing financial interest.

INTRODUCTION

Large defect-sized bone repair is a clinical challenge. Current treatment using allografts and autografts has met limitations with availability shortage, additional surgery, donor morbidity, disease transfer, immune reactions, and bacteria contamination.[1–4] Bone tissue engineering has emerged as a strategy to address these limitations by adopting external materials to help bridge the bone defect and facilitate bone regeneration.[5–7] Classic materials widely studied include metal implants, ceramic and bioglass stents, and polymeric scaffolds, which are expected to have good biocompatibility and help recruit stem cells or pre-osteoblasts to the surface.[2, 6–7] Cells adsorbed to the surface of the scaffolds will further undergo osteogenic differentiation and tissue mineralization to promote bone formation.[8]

Compared with implantation of pre-formed scaffolds, the minimally invasive injection route offers multiple advantages such as controllable injection volume, good adaptability to irregularly shaped defects, reduced surgical exposure with less pain, and faster recovery for patients.[9] In the past decades, various injectable systems, including liquid metal bone cements,[10] bioceramics and bioglass,[11] synthetic polymers, e.g., poly(methyl methacrylate) (PMMA), poly(ε-caprolactone) (PCL),[12] poly(L-lactic acid) (PLLA),[13] poly (propylene fumarate),[14] poly(ethylene glycol) (PEG),[15] and natural polymers, e.g., chitosan,[16] alginate,[17] were developed for bone regeneration. However, the degradation of these scaffold systems is a big concern. Most of the metal stents cannot be bio-adsorbed effectively and will remain in the body. For ceramics and bioglass implants, which may be adsorbed gradually *in vivo*, it is difficult to match the adsorption rate in sync with tissue formation. Polymeric scaffolds have additional concerns of immunogenicity or cytotoxicity of the chemicals used in the injectable system including pre-polymers, solvents, initiators, accelerators, and/or crosslinkable as well as the degradation products.

In recent years, the injectable, scaffolds-free biomimetic stem cell approach has started to gain intensive interest for bone regeneration.[18–21] Direct stem cell injection eliminates the concerns for biodegradation rate and biocompatibility of the injectable formulation and degradation products and saves a large amount of effort in refining the material formulations. In addition, instead of enlisting cells from the environment, the direct supply of stem cells to the defect sites shortens the time for cell recruitment and speeds up the regeneration process. With these advantages, various forms of stem cell injection, e.g., individual cells, cell sheets, and cell spheroids, have been reported for guiding tissue regenerations.[22–23] 3D cell spheroids can mimic key aspects of the native cellular microenvironment, and their uniform circular size suits perfectly for minimally invasive injection.[23] Spheroids generated with stem cells, e.g., mesenchymal stem cells (MSCs), has the ability to differentiate into multi-lineage cell types with corresponding induction.[24–27]

However, non-specific and uncontrolled differentiation of stem cells upon transplantation may not help specific tissue regeneration and even hinders therapeutic outcomes. Previous studies have showed that the transplantation of pure and non-differentiated MSCs failed to regenerate bone but instead resulted in fibrous tissue and adipose tissue formation.[28–29] Therefore, for bone tissue regeneration, stem cell transplantation often requires co-delivery of growth factors or biomaterials that can enhance osteogenic differentiation of stem cells to

bone cells.[30] To date, only limited studies have been reported to incorporate microparticles or nanomaterials into spheroids aiming at improving stem cell functions.[31–32]

Here, we propose a proof-of-concept strategy to incorporate cell-adhesion and osteogenic-instructive materials within stem cell spheroids to facilitate their aggregation and promote osteogenesis for bone tissue-engineering applications. We developed bone marrow mesenchymal stem cell (BMSC) spheroids that incorporated two-dimensional (2D) modular building blocks, e.g., hetero-nano-layers (2DHNL) composed of graphene oxide (GO) nanosheets and black phosphorus (BP) nanosheets, for enhanced *in vivo* bone regeneration, as demonstrated in Fig. 1a. We evaluated the effects of these engineered 2D materials on the proliferation and osteogenic differentiation of stem cells in a 3D spheroidal microenvironment. We further transplanted the engineered spheroids into rats and examined osteogenic differentiation of BMSCs and orthotopic bone regeneration in critical-sized calvarial defects. Finally, we introduced a combinational strategy by loading dexamethasone (DEX) on HNL to further support *in vivo* osteogenic induction and bone growth in rat calvarial defects. Altogether, the results obtained from the current study offer an operative scheme of inspirational stem cell/osteogenic factor co-delivery strategy using two-dimensional hetero-nano-layers for extensive bone defect repair (Fig. 1b).

RESULTS AND DISCUSSION

2D Materials Fabrication

As a star 2D nanomaterial, GO has gained broad interest for various biomedical applications taking advantage of its large surface area, outstanding mechanical properties (Young's modulus > 200 GPa for mono-layer GO), and strong protein adsorption abilities.[33–36] Atomic force microscopy (AFM) mapping showed the fabricated GO nanosheets had a height around 1 nm after exfoliation (Fig. 2a). This height is close to the layer height of GO, confirming the fabrication of mono-layer GO nanosheets.[37] Phosphorene, or commonly referred as BP in its multi-layered forms, is a biocompatible yet understudied 2D material with great potential in tissue engineering and other biomedical applications.[38–39] For exfoliated BP nanosheets, AFM imaging indicated small size flakes in the nanometer range with layer height around 31 nm (Fig. 2b), consistent with previous reports.[40–41] The detailed morphology of GO was observed to be thin layers by TEM scoping, as shown in Fig. 2c. BP nanosheets were observed by SEM and TEM to have lateral size around a few micrometers (Fig. 2d and Fig. S1a–b).

Here we combined the GO and BP to fabricate 2D hetero-nano-layer (2DHNL) nanostructures. The GO@BP HNL heterostructures were generated by mixing BP with GO under sonication. SEM imaging showed that the BP nanosheets were successfully wrapped by GO nanosheets (Fig. 2e). TEM images indicated that BP nanosheets were homogeneously distributed within the GO material (Fig. 2f). Enlarged scoping under TEM observed that BP nanosheets were covered by a large area of GO layer tightly (Fig. 2f). Element mapping of carbon and oxygen elements (main elements of GO) and phosphorous elements (main element of BP) further confirmed that BP nanosheets (green area) were widely dispersed with GO nanosheets (Fig. 2g). These SEM, TEM, and element mapping results indicate that BP nanosheets and GO nanosheets do not exclude each other and can

be combined to form heterostructure complexes. A schematic demonstration of the GO@BP HNL heterostructure is shown in Fig. 2h, with BP nanosheets and GO nanosheets mixed with each other.

GO nanosheets were widely reported to enhance cellular adhesion, spreading, proliferation, and differentiation.[42–43] Three-dimensional (3D) scaffolds functionalized with GO nanosheets were reported to promote epithelial genesis, adipogenesis, and osteogenesis of stem cells.[44–45] In addition to stem cells, GO nanosheets were also reported to support the differentiation and proliferation of multiple other cell types, including myoblasts and osteoblasts,[46–47] cardiomyocytes,[48–49] and neuronal cells.[50] For BP nanosheets, one of the most favored properties is its biodegradation products being phosphonates, which are common ions within the human body without any safety concerns.[41, 51] Phosphate is highly desired for the human skeleton and bone development as it plays an important role in osteogenesis and osteointegration.[52] These advantageous characteristics make phosphorene an interesting and promising 2D material for tissue engineering applications. However, the utilization of phosphate ions for tissue regeneration is still in its infancy.

Based on the successful fabrication of 2DHNL nanostructures, we tried to explore whether these materials can be incorporated within the stem cells to create functionalized spheroids. As shown in Fig. 2i, the SEM images showed 3D stem cell spheroids that are able to capture the nanomaterials within the spheroids. The spheroids incorporated with GO, BP, and GO@BP showed abundant extracellular matrix (ECM) development within the spheroids with tight cell-ECM and cell-cell contacts. For spheroids incorporated with BP or GO@BP HNL hetero-mixtures, distribution of BP nanosheets within the 3D spheroids was observed. These distributed BP nanosheets enabled individual stem cells to form interactions with them hence eliciting enhanced osteogenesis responses.

Functionalized Stem Cell Spheroid Formation

The cytotoxicity of GO and BP nanosheets to individual stem cells was evaluated by co-culturing with the cells at varying concentrations. As shown in Fig. 3a, with the increase of GO concentrations, cells showed lowered viabilities. A significant cytotoxic effect was observed at three days of co-culture with a GO concentration higher than 10 μg/mL. Instead of cytotoxicity, for BP nanosheets, an immediate enhancement of cell numbers at day 1 was determined at concentrations under 10 μg/mL (Fig. 3b). The enhanced cell proliferation was likely due to phosphate release to cell medium. However, with a concentration higher than 15 μg/mL, no obvious enhancement was observed, mostly because higher concentrations of phosphate ions and BP nanosheets disturbed normal cell activity. Significant cytotoxicities were determined when BP concentrations were higher than 20 μg/mL.

Cytotoxicity of GO and BP to 3D stem cell spheroids was evaluated by incorporating the nanosheets within the spheroids. The outcomes on spheroids shared similar trends with individual cells with slight difference. As shown in Fig. 3c, the incorporation of a small amount of BP nanosheets enhanced spheroid formation and stimulated the proliferation of cells to form larger-sized spheroids. The incorporation of GO nanosheets at an extremely low concentration of 4 μg/mL facilitated the formation of tight and uniform spheroids, taking advantage of the large area of GO. However, higher concentrations of GO caused

obvious toxicity to the spheroids, as can be seen from the increased dead cells from the spheroids (Fig. 3c and Fig. S2a–b). Based on these results, a concentration of 4 μg/mL was chosen for both GO and BP nanosheets for further spheroid formation and evaluation.

Photographs of 3D stem cell spheroids at day 1 showing the incorporation of GO nanosheets, BP nanosheets, and GO@BP hetero-mixtures are presented in Fig. 3d. Right after the addition of nanomaterials, the stem cells started to aggregate with the incorporated materials to form functionalized spheroids. Compared with pure spheroids, which form irregular shapes, the spheroids with GO, BP, or GO@BP HNL hetero-structures formed better round-ball-like spheroids. The cell-cell interactions and development of cellular filaments within the spheroids were observed on day 7 by immunofluorescent staining. As can be noted from Fig. 3e, at day 7, all spheroids were aggregated tightly to form uniform spheroids. An enlarged view of the cells within spheroids showed tight interactions between cells (Fig. 3e and Fig. S3a–b). All cells were tightly linked with each other to form integrated complexes. Robust intracellular filament developments were observed for all groups.

The DNA content in spheroids from day 1 till day 21 was monitored. As shown in Fig. 3f, the spheroids incorporated with BP or GO@BP hetero-mixtures showed a higher DNA content compared with the other groups. This may be due to the advantages of phosphate ion supply from the oxidation of BP nanosheets (Fig. 3g). The phosphate ion release kinetics of BP nanosheets at 1, 2, 4, 6, 8, 10, 14, and 21 days were determined. As can be noted from Fig. 3h, a burst release of phosphate ions was detected in the first 6 days. After that, the release reached a plateau region with mild but continuous release throughout the period of 21 days.

Phosphate ions (PO_4^{3-}) are acknowledged to help attract calcium ions (Ca^{2+}) to form calcium phosphate biominerals, which is important for late-stage bone formation.[53–54] The calcium depositions in the spheroids were visualized by calcein stain (green) and F-actin staining (red). As can be seen from the fluorescence images, the spheroids incorporated with either GO, BP, or GO@BP HNL materials showed obvious content of calcium biominerals deposition, stronger than the control group (Fig. 3i). This indicates that GO nanosheets can help to attract calcium ions and deposition of calcium phosphate biominerals (Fig. 3j).

In Vitro Osteogenesis of Spheroids

The osteogenesis of stem cell spheroids is critical for bone regeneration applications.[23–24, 32, 55–56] After incorporation of GO@BP HNL, the Sphero-HNL spheroids are slightly darker in color compared to the pure Sphero (Fig. 4a). To explore the osteogenesis ability of stem cells, spheroids were cultured in an osteogenic medium.

The quantitative analysis of mRNA expression of osteogenic markers osteopontin (OPN) and runt-related transcription factor 2 (Runx2) further confirmed the enhanced osteogenic differentiation of stem cells from BP nanosheets. As shown in Fig. 4b, the OPN expression levels in the Sphero-HNL is significantly higher than the other three groups. The Sphero-BP is significantly higher than the Sphero-GO and pure Sphero groups. The Runx2 mRNA

expression showed similar trends, with the highest expression detected in the Sphero-HNL group and Sphero-BP higher than the pure Sphero groups (Fig. 4c).

Immunofluorescence staining of OPN and Runx2 were conducted to confirm the osteogenic proteins expressions in stem cell spheroids. The OPN protein (green) was observed to be abundant in Sphero-BP and Sphero-HNL spheroids (Fig. 4d). As a comparison, lower content of OPN proteins was observed in the Sphero-GO group, with a negligible amount in the pure Sphero group. Further immunofluorescence staining of Runx2 showed its expression in all spheroids (Fig. 4e). However, a similar trend was observed that the highest protein contents were observed in the Sphero-HNL group. Obvious Runx2 protein was also observed in Sphero-GO and Sphero-BP groups at similar levels. Quantitative analysis of fluorescence intensity showed a significantly higher amount of OPN and Runx2 content for the Sphero-HNL group, as presented in Fig. 4f–g.

The intercellular OCN content was determined to be significantly higher for the spheroids incorporated with HNL at 14 and 21 days after induction (Fig. 4h). Interestingly, both sphero-GO and sphero-BP groups had higher OCN content than the pure Sphero group (Fig. 4h). The intracellular alkaline phosphatase (ALP) activity showed a significantly higher level at days 14 and 21 in spheroids incorporated with GO@BP HNL hetero-mixtures (Fig. 4i). The spheroid group that incorporated BP nanosheets also showed significantly higher ALP activity than the pure spheroids and the spheroids with GO nanosheets. These results indicate that both BP and GO nanosheets may facilitate the osteogenesis of stem cell spheroids, with a better effect observed for BP nanosheets over GO nanosheets. For the GO@BP HNL hetero-mixtures which contained both types of 2D materials, synergistic effects were exhibited to enhance osteogenesis to a significantly higher level.

To determine the *in vivo* biocompatibility of injected 3D stem cell spheroids and incorporated biomaterials, the organs of rats injected with or without 3D stem cell spheroids were sliced and analyzed by histological staining. As shown in Fig. 4j, no obvious damages were found in various organs from the rats, including the brain, spleen, kidney, liver, lung, and heart. This implies that the 3D stem cell spheroids and the incorporated biomaterials are biocompatible for *in vivo* injection.

Spheroids Enhanced *In Vivo* Bone Regeneration in Rat Calvarial Defect

To investigate the *in vivo* bone regeneration ability, the functionalized 3D stem cell spheroids were injected *in situ* to the critical-sized, 5-mm diameter cranial defect in rats (Fig. 5a–b). At 8 weeks post-surgery, bone regeneration in the defect site was evaluated by micro-CT and histology. As compared with the empty control, the micro-CT reconstruction images demonstrated that all bone defects injected with 3D stem cell spheroids had essential bone formation after 8 weeks (Fig. 5c). The maximal bone regeneration was observed for the Sphero-NHL group, with the largest bone piece forming over most of the defect area. The Sphero-BP group was also observed to have excellent regeneration ability, with large bone pieces closing the defect gap. Quantitative analysis of bone area showed the highest value at the bone defect site injected with spheroids incorporated with GO@BP HNL hetero-mixture (Fig. 5d). In addition, significantly higher bone area was determined for the Sphero-GO, Sphero-BP, and pure Sphero groups, as compared with the empty control without stem

cell spheroid injection. Characterization of bone volume to tissue volume (BV/TV) ratio confirmed a similar trend with the highest BV/TV ratio detected in the Sphero-HNL group (Fig. 5e). Meanwhile, the Sphero-BP, Sphero-GO, Sphero-BP, and pure Sphero groups all showed higher BV/TV ratios than the empty control group without stem cell spheroids. The bone mineral density (BMD) in the defect site was further calculated. As shown in Fig. 5f, BMD values were significantly higher in the Sphero-BP and Sphero-HNL groups. These results indicate that the stem cell spheroids can enhance bone formation *in vivo*. The addition of either BP or GO nanosheets may facilitate the bone formation, with positive synergistic effects observed for GO@BP HNL hetero-mixtures.

Histological analysis was conducted to further evaluate the bone formation pattern in the defect sites. As shown in Fig. 5g, H&E staining showed that only thin layers of tissue were developed in the empty control group without spheroids. In contrast, a thicker tissue layer was observed in the bone defects injected with 3D stem cell spheroids. In addition, for the empty control, the bone defect was stained to be largely fibrous tissue without essential bone development. For bone defect injected with Sphero-HNL, obvious bone tissue was stained as compared to the other groups. Further toluidine blue staining (Fig. S4) and Masson trichrome staining (Fig. S5) showed a similar trend of larger bone formation in the defect area injected with spheroids incorporated with GO@BP HNL nanostructures.

In Vivo Osteogenesis and Neovascularization

The *in vivo* neovascularization and osteogenesis in the bone defect were detected by real-time quantitative polymerase chain reaction (real-time PCR) and immunofluorescence co-staining. As shown in Fig. 6a–c, significantly higher levels of osteogenesis marker expression were quantified for spheroids with GO, BP, and GO@BP HNL hetero-mixtures, as compared with the empty control and pure stem cell spheroids. Further, the highest ALP activity was determined in defects injected with spheroids incorporated with GO@BP HNL hetero-mixtures (Fig. 6d). The protein content for CD31 (vascular marker) and ALP (osteogenesis marker) were visualized by immunofluorescence co-staining. Results showed abundant ALP and CD31 expression in the bone defect area injected with 3D stem cell spheroids (Fig. 6e–f and Fig. S6). The strongest staining was observed in the defect area injected with spheroids incorporated with GO@BP HNL hetero-mixtures. As a comparison, the empty control group was largely stained with blue (cell nuclei) and showed a much lower content of ALP and CD31 proteins. An enlarged view of the detailed distribution of ALP and CD31 proteins in the defect area showed that the CD31 vascular marker was mainly deposited in the wall of sparsely distributed blood vessels. In contrast, the ALP protein showed main development surrounding the bone area, as indicated in Fig. 6e–f. Quantitative analysis of fluorescence intensity showed a significantly higher amount of ALP and CD31 for the Sphero-HNL group, as presented in Fig. 6g–h.

These results indicate that the injectable 3D stem cell spheroids could facilitate *in-situ* neovascularization and osteointegration, which further enhance bone formation (Fig. 6i). The outcomes are consistent with previous reports that the incorporation of bone proteins or osteogenic nanocomponents may enhance cell osteogenesis *in vitro* and bone regeneration *in vivo*. For example, the addition of bone morphogenetic protein-2 (BMP-2) loaded

microparticles in mesenchymal stem cell aggregates significantly promoted osteogenic differentiation of hMSCs for bone tissue engineering.[56] Furthermore, the incorporation of mineral-coated hydroxyapatite or fibers coated with adenosine within stem cell aggregates enhanced osteogenesis.[23, 55]

In Vivo Stem Cell and Osteogenic Factor Co-Delivery for Combinational Therapy

The osteogenesis of stem cells can be achieved by *in vitro* induction using a medium containing both phosphate and DEX for 14 days (Fig. 7a). However, this induction costs extra incubation time. In addition, the cells in the center of spheroids may not have effective access to the induction medium thus not undergo osteogenesis as expected. Furthermore, these cells may stop growing or even die due to the lack of access to oxygen and nutrients during the long induction period.

To overcome these challenges, we incorporated the osteogenic induction compounds within the stem cell spheroids which could induce osteogenesis from the beginning, as demonstrated in Fig. 7b. Since there is already phosphate supply from the black phosphorus nanosheets, we only need to incorporate DEX in the GO@BP HNL hetero-structures. Taking advantage of the large surface area of GO nanosheets, the DEX may be loaded by pi-pi stacking under sonication, as illustrated in Fig. 7c. The release kinetics showed that the DEX had burst release in 4 days if loaded on the BP nanosheets, possibly due to the fast oxidation of BP nanosheets, thus causing the release of surficial DEX molecules. In comparison, DEX loaded into GO@BP HNL hetero-mixtures maintained sustained release during a period of 21 days, as shown in Fig. 7d. This trend may have resulted from synergistic contributions from the fast release from BP nanosheets and slow release from the GO nanosheets.

Immunofluorescence staining showed that the stem cell spheroids with HNL had essential Runx2 osteogenic marker expression after induction for 14 days in an osteogenic medium (Fig. 7e). On the other hand, the spheroids incorporated with HNL-DEX showed comparable Runx2 osteogenic marker expression after incubation purely in a regular non-osteogenesis medium, as can be seen in Fig. 7f. The mRNA expression analysis showed essential expression of osteogenic markers OPN and Osterix (OSX) in Sphero-HNL after induction in osteogenic medium. The level of these osteogenic markers in Sphero-HNL-DEX were tested to be comparable to that of Sphero-HNL after induction, as shown in Fig. 7g–h. These results indicate that the HNL-DEX nanosheets with sustained release of phosphate ions and DEX molecules could induce stem cell differentiation toward an osteogenic trend.

The *in vivo* bone repair capability of DEX incorporated spheroids was evaluated using a rat cranial defect model. After 4 weeks of implantation, the micro-CT reconstruction images showed comparable bone regeneration with both Sphero-HNL after 14 days of osteo-medium induction and direct Sphero-HNL-DEX implantation without induction. Quantitative analysis showed close values in bone area, BV/TV ratio, and BMD for the two groups (Fig. 7j–l). Both groups had significant bone formation compared to the empty control without spheroid implantation (Fig. 7j–l).

Histological analysis was further conducted to evaluate the bone regeneration pattern in the defect sites. As shown in Fig. 7m, the H&E staining showed an only thin layer of fibrous tissue was developed in the empty control group without spheroids. In contrast, thicker tissue and bone were observed in the bone defects injected with either Sphero-HNL with 14 days of osteo-medium induction or Sphero-HNL-DEX with direct implantation. Further toluidine blue staining and Masson trichrome staining demonstrated a similar trend of comparable bone formation in the defect area injected with the two types of stem cell spheroids.

The *in vivo* neovascularization and osteogenesis in the defect sites were analyzed by PCR and immunofluorescence co-staining. As shown in Fig. 8a–c, significantly higher levels of osteogenesis marker expression were quantified for the two spheroid groups compared with the empty control. Further, the vascular marker CD31 protein and osteogenesis marker ALP protein was visualized by immunofluorescence staining. As shown in Fig. 8d–e, abundant ALP and CD31 expression were observed in the bone defect area injected with either Sphero-HNL with 14 days of osteogenic medium induction or Sphero-HNL-DEX with direct implantation, both significantly higher than the empty control. As can be seen from the fluorescence images in Fig. 8f, the strongest ALP and CD31 fluorescence was observed in the defect area injected with spheroids incorporated with GO@BP HNL hetero-mixtures. An enlarged view of the detailed distribution of CD31 proteins in the defect area showed these proteins were mainly deposited in the wall of sparsely distributed blood vessels. In contrast, the enlarged view of ALP protein showed the main development surrounding the bone area. As a comparison, the empty control group was largely stained with blue (cell nuclei) and had a much lower content of CD31 and ALP protein. These results indicate that both injectable Sphero-HNL with 14 days osteogenic medium induction and Sphero-HNL-DEX with direct implantation could facilitate *in-situ* neovascularization development and osteointegration, and subsequent bone formation.

DEX has been widely utilized to induce the osteogenesis of mesenchymal stem/progenitor cells. The *in vivo* animal studies also demonstrated that DEX could facilitate the formation of callus and stimulate bone bridging in the bone defect area.[57] In addition, DEX incorporated mesoporous silica nanoparticles were reported to stimulate osteogenic differentiation of stem cells with elevated ALP activity, calcium deposition, and bone-related protein expressions. The *in vivo* intramuscular implantation of these DEX incorporated nanoparticles in rats for 3 weeks showed effective osteogenesis and bone regeneration, as confirmed by both computed tomography (CT) and histological analysis.[58] In the current study, DEX incorporated with 2D materials further confirmed that DEX delivery enhanced the *in vitro* cell osteogenesis and *in vivo* bone regeneration.

Previous work has reported that both BP nanosheets and GO nanosheets are able to facilitate bone cell proliferation and osteogenesis on hydrogels and 3D printed scaffolds.[59–62] The outcomes from the current work demonstrated that the 2D hetero-nano-layered materials containing BP nanosheets and GO nanosheets are able to embed into the stem cell spheroids and enhance the osteogenic induction *in vitro*. Cell and animal studies also demonstrated that the 2D hetero-nano-layered materials were able to serve as carriers for osteogenic factors delivery and enhance osteogenesis and neovascularization *in vivo* for bone tissue

regeneration. These results indicate that the 2D hetero-nano-layered materials are promising as delivery carriers for bioactive molecules for various biomedical applications.

CONCLUSION

In summary, we engineered functional spheroids with MSCs embedded with 2D black phosphorus and graphene oxide (blended 2DHNL) to create a 3D cell-instructive microenvironment for bone repair. The biocompatibility and effects of the engineered 2D materials on the proliferation and osteogenic differentiation of stem cells were evaluated in an *in vitro* 3D spheroidal microenvironment. The *in vivo* study by transplanting these engineered spheroids into rat calvarial defects showed excellent support of osteogenic differentiation of MSCs with essential bone regeneration. Immunofluorescence staining of vascular marker CD31 and osteogenic marker ALP indicated the 3D stem cell spheroids could facilitate in-situ osteointegration and neovascularization in bone defects. Loading of osteogenic inductive factor DEX on the 2DHNL allowed internal osteogenic induction without prior incubation in the osteogenic medium. The shortened overall culture time offers a great advantage for clinical translation. These 2DHNL embedded functional stem cell spheroids, with phosphate and osteogenic induction factor co-delivery capability, could provide cells and differentiation clues in an all-in-one system to create large tissues in a time-effective manner, thus are promising for large bone defect repair.

EXPERIMENTAL SECTION

Fabrication of BP and GO Nanosheets

BP nanosheets were fabricated by liquid exfoliation as described previously.[40, 63] Briefly, 30 mg of BP powder (ACS Material, LLC, Pasadena, CA) was sonicated for 1 hour using a probe model sonicator (Qsonica Q500) in 30 mL deionized (DI) H_2O followed by 12 hours of sonication in an ice bath sonicator (Elmasonic S10, Elma Schmidbauer GmbH, Germany). Unexfoliated BP powder was removed by centrifugation (5000 rpm, 10 min), and the BP nanosheets in the supernatant were collected. GO nanosheets were exfoliated from natural graphite (~150 μm flakes, Sigma Aldrich, Milwaukee, WI) using an improved Hummers' method, as described previously.[37] The GO@BP hetero-nano-layers were fabricated by mixing BP nanosheets and GO nanosheets followed by sonication for 5 min in an aqueous solution.

Cytotoxicity Screening and Spheroid Biocompatibility

Rat bone marrow-derived mesenchymal stem cells (rBMSCs) (Sprague-Dawley, Fisher Scientific, PA) were cultured in low glucose Dulbecco's Modified Eagle's Medium (DMEM, Gibco, Carlsbad, CA) supplemented with 0.5% penicillin-streptomycin (Pen-Strep, Gibco) and 10% fetal bovine serum (FBS, Gibco) in a 37 °C cell incubator (5% CO2, 95% relative humidity). Prior to cell studies, the exfoliated 2D materials solution were further sonicated for 1 hour and placed under UV for 30 min for full dispersion and sterilization. To determine the cytotoxicities of GO nanosheets and BP nanosheets, rBMSCs were co-cultured with varied concentrations of GO and BP nanosheets for 3 days. The rBMSC cell numbers in

each treatment were determined using the MTS assay, and cell viability was calculated by normalizing to tissue culture polystyrene (TCPS) positive control (set as 100%).

For the spheroid viability study, rBMSCs were trypsinized from a cell culture flask, counted, centrifuged, and resuspended to a final concentration of 4×10^5 cells/mL in a culture medium containing varying concentrations of GO nanosheets and BP nanosheets. Corning spheroid microplates (Corning, Arizona) were used to form the spheroids by adding 50μL cell solution to each well with individual spheroids consisting of 2×10^4 cells. The microplate with cells was centrifuged gently for 5 minutes at 1500 rpm before culture in the incubator. After 3 days of culture, the cell viability in spheroids was determined by staining with the LIVE/DEAD® Cell Imaging Kit (Thermo Fisher Scientific, Waltham, MA) and scoped on an inverted laser scanning confocal microscope (Carl Zeiss, Germany).

Functionalized Spheroid Formation

The rBMSCs were trypsinized from cell culture flask and resuspended to a final concentration of 4×10^5 cells/mL in four types of culture medium: 1) pure medium, 2) medium containing 4 μg/mL GO nanosheets, 3) medium containing 4 μg/mL BP nanosheets, and 4) medium containing 4 μg/mL GO nanosheets and 4 μg/mL BP nanosheets. Corning spheroid microplates were used to form the spheroids by adding 50μL cell solution to each well with individual spheroids consisting of 2×10^4 cells. The microplate with cells was centrifuged gently for 5 minutes at 1500 rpm before culture in the incubator. After 1 day of spheroid formation, the medium was gently replaced with osteogenic medium supplemented with 10 mM β-glycerophosphate sodium, 50 μg/mL ascorbic acid (AA), and 10 nM dexamethasone (DEX) (Sigma-Aldrich Co., Milwaukee, WI). After 3 days of culture, the spheroids were fixed in 4% paraformaldehyde (PFA) solution and dehydrated by critical point drying. After being mounted on an aluminum stub and sputter-coated with gold-palladium, the morphological structures of spheroids were observed on a scanning electron microscope (S-4700, Hitachi Instruments, Tokyo, Japan).

Cellular Filaments and DNA Contents in Spheroids

Fixed spheroids were washed with PBS, permeabilized with 0.2% Triton X-100, and stained with rhodamine-phalloidin (RP, Cytoskeleton Inc, Denver, CO) and 4’,6-diamidino-2-phenylindole (DAPI). Fluorescence-labeled rBMSC spheroids were imaged on a laser scanning confocal microscope (Carl Zeiss, Germany). The dsDNA in spheroids was extracted using 200μL pureTRIzol (Bio-Rad, Hercules, CA, U.S.A.) and 40μL chloroform. After centrifuging for 10 min at 12000 rpm, the dsDNA pellets were washed with 75% (v/v) ethanol, dried, and redissolved in double-distilled water. The concentrations of extracted dsDNA were detected by NanoDrop 2000 Spectrophotometer (Thermo Fisher Scientific, Waltham, MA, U.S.A.).

Phosphate Ion Release and Calcium Deposition in Spheroids

The phosphate ion release kinetics from spheroids was determined using the phosphate assay kit (ab65622, Abcam, Cambridge, UK) according to the kit protocol. After fixation, the minerals deposited in spheroids were stained with 50 μM calcein solution, and filaments

in cells were stained with rhodamine-phalloidin. The stained minerals and cells in spheroids were scoped on an inverted laser scanning confocal microscope.

Osteogenesis Biomarker Expression and Staining in Spheroids

The mRNA expression level of osteogenic markers was quantified by real-time PCR using rat-specific primers (Table S1). After being cultured for 14 days, the stem cell spheroids were fixed for 1 hour with 4% PFA solution and then permeabilized by 0.2% Triton X-100 solution for another hour. Fixed spheroids were incubated with 3% bovine serum albumin (BSA)/PBS solution to block non-specific binding sites at 37 °C for 30 minutes. To stain the osteogenic markers, the spheroids were incubated with anti-Runt-related transcription factor 2 (Runx2) antibody (1:100 in PBS, Abcam, ab23981) or anti-osteopontin (OPN) antibody (1:100 in PBS, Abcam, ab8448) overnight at 4°C. A secondary goat anti-rabbit IgG (Alexa Fluor 488, Abcam, ab150077) was used to label the osteogenic proteins by incubation for 2 hours. After the staining, spheroids were further stained with 4’,6-diamidino-2-phenylindole (DAPI) at 37 °C for 10 min to label cell nuclei. The immunofluorescence labeled spheroids were visualized by a LSM 780 Zeiss Confocal Microscope. Fluorescence intensities were analyzed by the ImageJ software.

Alkaline Phosphatase (ALP) Activity and Osteocalcin (OCN)

Functionalized spheroids were lysed in 0.2% Triton X-100 solution for 30 minutes, and the ALP concentration was quantified using a QuantiChrome™ Alkaline Phosphatase Assay Kit (DALP-250, BioAssay Systems, Hayward, CA) according to the protocol instructions. The OCN concentration in the spheroids culture medium was quantified by the Rat Osteocalcin Enzyme Immunoassay Kit (Alfa Aesar, Haverhill, MA) and calculated using a standard curve method according to the standard concentrations provided by the kit.[64]

In Vivo Bone Regeneration of Spheroids in Rat

All animal work in the current study was performed in accordance with the Institutional Animal Care and Use Committee (IACUC) of Mayo Clinic, Rochester, MN. Two critical-sized cranial defects of 5-mm diameter were created on both sides of the skull in the Sprague Dawley rats.[65–67] The four types of spheroids with varied components were dispersed in 100 μl sterilized saline solution at a concentration of 20 spheroids per formulation. The saline with spheroids was then transferred into a 1 mL syringe and injected to the defect immediately. Empty defects without spheroids served as control. The skin of defects was closed with non-resorbable 4–0 Vicryl sutures. Each formulation was studied by three replicates. After 8 weeks of implantation, rats were sacrificed, and cranial defect tissues were fixed for 1 day in 10% PFA solution and scanned on a micro-CT system (Bruker Skyscan 1276, Germany).

In Vivo Osteogenesis and Neovascularization of Stem Cell Spheroids

Rat defects were decalcified in EDTA hydrochloric acid decalcifying solution (Thermo Fisher Scientific) then embedded in paraffin and sliced. Histological staining with H&E, toluidine blue, and Masson trichrome staining was conducted and scoped by a scanner (AxioScan Z1, Carl Zeiss, Germany). *In vivo* neovascularization and osteogenesis in

the bone defects were analyzed by immunofluorescence co-staining of CD31 (Novus Biologicals, USA) and ALP (Novus Biologicals, USA) with observation using a laser scanning confocal microscope.

In Vivo Osteogenesis and Bone Repair Combinational Therapy

Spheroids with DEX loaded GO@BP hetero-nano-layer.—The GO@BP-DEX hetero-nano-layer was fabricated by mixing of BP nanosheets, GO nanosheets, and dexamethasone solution followed by sonication for 5 min. The release kinetic of DEX from GO@BP-DEX hetero-nano-layers was carried out in PBS solution (pH 7.4) and monitored via UV−vis spectra at 242 nm. Stem cell spheroids incorporated with GO@BP-DEX hetero-nano-layer were fabricated using the corning spheroid microplates (Corning, Arizona) with the same procedures as described above. Immunofluorescence staining and mRNAs expression detection in spheroids with GO@BP-DEX hetero-nano-layer were carried out using similar procedures.

***In vivo* bone repair.—**Animal work was conducted using Sprague Dawley rats with two critical-sized cranial defects of 5-mm diameter on both sides of the skull. Spheroids with GO@BP induced for 14 days in osteogenic medium and spheroids with GO@BP-DEX hetero-nano-layer without *in vitro* induction were implanted into the defects. Empty defects without spheroids served as control. The skin of defects was closed with non-resorbable 4–0 Vicryl sutures. Each formulation was studied by three replicates. After 4 weeks of implantation, rats were sacrificed, and cranial defect tissues were fixed for 1 day in 10% PFA solution and scanned on a micro-CT system

Immunohistology analysis.—The rat cranial defects were decalcified in EDTA hydrochloric acid decalcifying solution. After being embedded in paraffin, the tissues were sliced and stained with H&E, toluidine blue, and Masson trichrome staining then scoped by a scanner. *In vivo* neovascularization and osteogenesis in the bone defects were analyzed by immunofluorescence staining of ALP and CD31.

Statistical Analysis

Statistical analysis of data was conducted by one-way analysis of variance (ANOVA) followed by Tukey’s post-test. Groups with p values less than 0.05 were marked as significantly different.

Supplementary Material

Refer to Web version on PubMed Central for supplementary material.

ACKNOWLEDGMENTS

This work was supported by the National Institutes of Health grant R01 AR075037. The micro-CT work was supported in part by the Mayo Clinic X-ray Imaging Core.

REFERENCES

(1). Koons GL; Diba M; Mikos AG, Materials Design for Bone-Tissue Engineering. Nat. Rev. Mater 2020, 5 (8), 584–603.

(2). Ogueri KS; Laurencin CT, Nanofiber Technology for Regenerative Engineering. ACS Nano 2020, 14 (8), 9347–9363. [PubMed: 32678581]

(3). Hu C; Ashok D; Nisbet DR; Gautam V, Bioinspired Surface Modification of Orthopedic Implants for Bone Tissue Engineering. Biomaterials 2019, 219, 119366. [PubMed: 31374482]

(4). Oryan A; Alidadi S; Moshiri A; Maffulli N, Bone Regenerative Medicine: Classic Options, Novel Strategies, and Future Directions. J. Orthop. Surg. Res 2014, 9 (1), 1–27. [PubMed: 24383821]

(5). Zhao Z; Li G; Ruan H; Chen K; Cai Z; Lu G; Li R; Deng L; Cai M; Cui W, Capturing Magnesium Ions Via Microfluidic Hydrogel Microspheres for Promoting Cancellous Bone Regeneration. ACS Nano 2021, 15 (8), 13041–13054.

(6). De Witte T-M; Fratila-Apachitei LE; Zadpoor AA; Peppas NA, Bone Tissue Engineering Via Growth Factor Delivery: From Scaffolds to Complex Matrices. Regen. Biomater 2018, 5 (4), 197–211. [PubMed: 30094059]

(7). Bose S; Roy M; Bandyopadhyay A, Recent Advances in Bone Tissue Engineering Scaffolds. Trends Biotechnol 2012, 30 (10), 546–554. [PubMed: 22939815]

(8). Wubneh A; Tsekoura EK; Ayranci C; Uludağ H, Current State of Fabrication Technologies and Materials for Bone Tissue Engineering. Acta Biomater 2018, 80, 1–30. [PubMed: 30248515]

(9). Salgado CL; Sanchez EM; Zavaglia CA; Almeida AB; Granja PL, Injectable Biodegradable Polycaprolactone-Sebacic Acid Gels for Bone Tissue Engineering. Tissue Eng. Part A 2012, 18 (1–2), 137–46. [PubMed: 21902607]

(10). Sun X; Yuan B; Sheng L; Rao W; Liu J, Liquid Metal Enabled Injectable Biomedical Technologies and Applications. Appl. Mater. Today 2020, 20, 100722.

(11). Zhu Y; Kong L; Farhadi F; Xia W; Chang J; He Y; Li H, An Injectable Continuous Stratified Structurally and Functionally Biomimetic Construct for Enhancing Osteochondral Regeneration. Biomaterials 2019, 192, 149–158. [PubMed: 30448699]

(12). Liu X; Camilleri ET; Li L; Gaihre B; Rezaei A; Park S; Miller II AL; Tilton M; Waletzki BE; Terzic A, Injectable Catalyst-Free “Click” Organic-Inorganic Nanohybrid (Click-on) Cement for Minimally Invasive in Vivo Bone Repair. Biomaterials 2021, 276, 121014. [PubMed: 34280821]

(13). Lasprilla AJ; Martinez GA; Lunelli BH; Jardini AL; Maciel Filho R, Poly-Lactic Acid Synthesis for Application in Biomedical Devices—A Review. Biotechnol. Adv 2012, 30 (1), 321–328. [PubMed: 21756992]

(14). Liu X; Miller AL; Xu H; Waletzki BE; Lu L, Injectable Catalyst-Free Poly (Propylene Fumarate) System Cross-Linked by Strain Promoted Alkyne–Azide Cycloaddition Click Chemistry for Spine Defect Filling. Biomacromolecules 2019, 20 (9), 3352–3365. [PubMed: 31398020]

(15). Neumann AJ; Quinn T; Bryant SJ, Nondestructive Evaluation of a New Hydrolytically Degradable and Photo-Clickable Peg Hydrogel for Cartilage Tissue Engineering. Acta Biomater 2016, 39, 1–11. [PubMed: 27180026]

(16). LogithKumar R; KeshavNarayan A; Dhivya S; Chawla A; Saravanan S; Selvamurugan N, A Review of Chitosan and Its Derivatives in Bone Tissue Engineering. Carbohydr. Polym 2016, 151, 172–188. [PubMed: 27474556]

(17). Pina S; Oliveira JM; Reis RL, Natural-Based Nanocomposites for Bone Tissue Engineering and Regenerative Medicine: A Review. Adv. Mater 2015, 27 (7), 1143–1169. [PubMed: 25580589]

(18). Fernandez-Yague MA; Abbah SA; McNamara L; Zeugolis DI; Pandit A; Biggs MJ, Biomimetic Approaches in Bone Tissue Engineering: Integrating Biological and Physicomechanical Strategies. Adv. Drug Deliv. Rev 2015, 84, 1–29. [PubMed: 25236302]

(19). Ng J; Spiller K; Bernhard J; Vunjak-Novakovic G, Biomimetic Approaches for Bone Tissue Engineering. Tissue Eng. Part B Rev 2017, 23 (5), 480–493. [PubMed: 27912680]

(20). Ovsianikov A; Khademhosseini A; Mironov V, The Synergy of Scaffold-Based and Scaffold-Free Tissue Engineering Strategies. Trends Biotechnol 2018, 36 (4), 348–357. [PubMed: 29475621]

(21). Herberg S; Varghai D; Alt DS; Dang PN; Park H; Cheng Y; Shin J-Y; Dikina AD; Boerckel JD; Rolle MW; Alsberg E, Scaffold-Free Human Mesenchymal Stem Cell Construct Geometry Regulates Long Bone Regeneration. Commun. Biol 2021, 4 (1), 1–16. [PubMed: 33398033]

(22). Guven S; Chen P; Inci F; Tasoglu S; Erkmen B; Demirci U, Multiscale Assembly for Tissue Engineering and Regenerative Medicine. Trends Biotechnol 2015, 33 (5), 269–279. [PubMed: 25796488]

(23). Ahmad T; Byun H; Lee J; Perikamana SKM; Shin YM; Kim EM; Shin H, Stem Cell Spheroids Incorporating Fibers Coated with Adenosine and Polydopamine as a Modular Building Blocks for Bone Tissue Engineering. Biomaterials 2020, 230, 119652. [PubMed: 31787333]

(24). Lin H; Li Q; Lei Y, Three-Dimensional Tissues Using Human Pluripotent Stem Cell Spheroids as Biofabrication Building Blocks. Biofabrication 2017, 9 (2), 025007. [PubMed: 28287080]

(25). Cheng N-C; Wang S; Young T-H, The Influence of Spheroid Formation of Human Adipose-Derived Stem Cells on Chitosan Films on Stemness and Differentiation Capabilities. Biomaterials 2012, 33 (6), 1748–1758. [PubMed: 22153870]

(26). Edmondson R; Broglie JJ; Adcock AF; Yang L, Three-Dimensional Cell Culture Systems and Their Applications in Drug Discovery and Cell-Based Biosensors. Assay Drug Dev. Techno 2014, 12 (4), 207–218.

(27). Lee J; Jeon O; Kong M; Abdeen AA; Shin J-Y; Lee HN; Lee YB; Sun W; Bandaru P; Alt DS, Combinatorial Screening of Biochemical and Physical Signals for Phenotypic Regulation of Stem Cell–Based Cartilage Tissue Engineering. Sci. Adv 2020, 6 (21), eaaz5913. [PubMed: 32494742]

(28). Hu L; Yin C; Zhao F; Ali A; Ma J; Qian A, Mesenchymal Stem Cells: Cell Fate Decision to Osteoblast or Adipocyte and Application in Osteoporosis Treatment. Int. J. Mol. Sci 2018, 19 (2), 360.

(29). Winkler T; Sass F; Duda G; Schmidt-Bleek K, A Review of Biomaterials in Bone Defect Healing, Remaining Shortcomings and Future Opportunities for Bone Tissue Engineering: The Unsolved Challenge. Bone Joint Res 2018, 7 (3), 232–243. [PubMed: 29922441]

(30). James AW, Review of Signaling Pathways Governing Msc Osteogenic and Adipogenic Differentiation. Scientifica 2013, 2013.

(31). Bratt-Leal AM; Carpenedo RL; Ungrin MD; Zandstra PW; McDevitt TC, Incorporation of Biomaterials in Multicellular Aggregates Modulates Pluripotent Stem Cell Differentiation. Biomaterials 2011, 32 (1), 48–56. [PubMed: 20864164]

(32). Ahmad T; Shin HJ; Lee J; Shin YM; Perikamana SKM; Park SY; Jung HS; Shin H, Fabrication of in Vitro 3d Mineralized Tissue by Fusion of Composite Spheroids Incorporating Biomineral-Coated Nanofibers and Human Adipose-Derived Stem Cells. Acta Biomater 2018, 74, 464–477. [PubMed: 29803004]

(33). Chung C; Kim Y-K; Shin D; Ryoo S-R; Hong BH; Min D-H, Biomedical Applications of Graphene and Graphene Oxide. Accounts Chem. Res 2013, 46 (10), 2211–2224.

(34). Georgakilas V; Tiwari JN; Kemp KC; Perman JA; Bourlinos AB; Kim KS; Zboril R, Noncovalent Functionalization of Graphene and Graphene Oxide for Energy Materials, Biosensing, Catalytic, and Biomedical Applications. Chem. Rev 2016, 116 (9), 5464–5519. [PubMed: 27033639]

(35). Suk JW; Piner RD; An J; Ruoff RS, Mechanical Properties of Monolayer Graphene Oxide. ACS Nano 2010, 4 (11), 6557–6564. [PubMed: 20942443]

(36). Seaberg J; Montazerian H; Hossen MN; Bhattacharya R; Khademhosseini A; Mukherjee P, Hybrid Nanosystems for Biomedical Applications. ACS Nano 2021, 15 (2), 2099–2142. [PubMed: 33497197]

(37). Marcano DC; Kosynkin DV; Berlin JM; Sinitskii A; Sun Z; Slesarev A; Alemany LB; Lu W; Tour JM, Improved Synthesis of Graphene Oxide. ACS Nano 2010, 4 (8), 4806–4814. [PubMed: 20731455]

(38). Liu X; Gaihre B; George MN; Li Y; Tilton M; Yaszemski MJ; Lu L, 2D Phosphorene Nanosheets, Quantum Dots, Nanoribbons: Synthesis and Biomedical Applications. Biomater. Sci 2021, 9, 2768–2803. [PubMed: 33620047]

(39). Xia F; Wang H; Hwang JC; Neto AC; Yang L, Black Phosphorus and Its Isoelectronic Materials. Nat. Rev. Phys 2019, 1 (5), 306–317.

(40). Chen L; Zhou G; Liu Z; Ma X; Chen J; Zhang Z; Ma X; Li F; Cheng HM; Ren W, Scalable Clean Exfoliation of High-Quality Few-Layer Black Phosphorus for a Flexible Lithium Ion Battery. Adv. Mater 2016, 28 (3), 510–517. [PubMed: 26584241]

(41). Dhanabalan SC; Ponraj JS; Guo Z; Li S; Bao Q; Zhang H, Emerging Trends in Phosphorene Fabrication Towards Next Generation Devices. Adv. Sci 2017, 4 (6), 1600305.

(42). Lee WC; Lim CHY; Shi H; Tang LA; Wang Y; Lim CT; Loh KP, Origin of Enhanced Stem Cell Growth and Differentiation on Graphene and Graphene Oxide. ACS Nano 2011, 5 (9), 7334–7341. [PubMed: 21793541]

(43). Xia Y; Yang H; Li S; Zhou S; Wang L; Tang Y; Cheng C; Haag R, Multivalent Polyanionic 2d Nanosheets Functionalized Nanofibrous Stem Cell-Based Neural Scaffolds. Adv. Funct. Mater 2021, 31 (20), 2010145.

(44). Luo Y; Shen H; Fang Y; Cao Y; Huang J; Zhang M; Dai J; Shi X; Zhang Z, Enhanced Proliferation and Osteogenic Differentiation of Mesenchymal Stem Cells on Graphene Oxide-Incorporated Electrospun Poly (Lactic-Co-Glycolic Acid) Nanofibrous Mats. ACS Appl. Mater. Interfaces 2015, 7 (11), 6331–6339. [PubMed: 25741576]

(45). Kim J; Choi KS; Kim Y; Lim KT; Seonwoo H; Park Y; Kim DH; Choung PH; Cho CS; Kim SY, Bioactive Effects of Graphene Oxide Cell Culture Substratum on Structure and Function of Human Adipose-Derived Stem Cells. J. Biomed. Mater. Res. A 2013, 101 (12), 3520–3530. [PubMed: 23613168]

(46). Depan D; Girase B; Shah J; Misra R, Structure–Process–Property Relationship of the Polar Graphene Oxide-Mediated Cellular Response and Stimulated Growth of Osteoblasts on Hybrid Chitosan Network Structure Nanocomposite Scaffolds. Acta Biomater 2011, 7 (9), 3432–3445. [PubMed: 21664303]

(47). Ku SH; Park CB, Myoblast Differentiation on Graphene Oxide. Biomaterials 2013, 34 (8), 2017–2023. [PubMed: 23261212]

(48). Shin SR; Aghaei-Ghareh-Bolagh B; Dang TT; Topkaya SN; Gao X; Yang SY; Jung SM; Oh JH; Dokmeci MR; Tang X, Cell-Laden Microengineered and Mechanically Tunable Hybrid Hydrogels of Gelatin and Graphene Oxide. Adv. Mater 2013, 25 (44), 6385–6391. [PubMed: 23996513]

(49). Cha C; Shin SR; Gao X; Annabi N; Dokmeci MR; Tang X; Khademhosseini A, Controlling Mechanical Properties of Cell-Laden Hydrogels by Covalent Incorporation of Graphene Oxide. Small 2014, 10 (3), 514–523. [PubMed: 24127350]

(50). Liu X; Miller AL; Park S; Waletzki BE; Zhou Z; Terzic A; Lu L, Functionalized Carbon Nanotube and Graphene Oxide Embedded Electrically Conductive Hydrogel Synergistically Stimulates Nerve Cell Differentiation. ACS Appl. Mater. Interfaces 2017, 9 (17), 14677–14690. [PubMed: 28406608]

(51). Shao J; Xie H; Huang H; Li Z; Sun Z; Xu Y; Xiao Q; Yu X-F; Zhao Y; Zhang H; Wang H; Chu PK, Biodegradable Black Phosphorus-Based Nanospheres for in Vivo Photothermal Cancer Therapy. Nat. Commun 2016, 7, 12967. [PubMed: 27686999]

(52). Wang X; Shao J; El Raouf MA; Xie H; Huang H; Wang H; Chu PK; Yu X-F; Yang Y; AbdEl-Aal AM, Near-Infrared Light-Triggered Drug Delivery System Based on Black Phosphorus for in Vivo Bone Regeneration. Biomaterials 2018, 179, 164–174. [PubMed: 29986234]

(53). Huang K; Wu J; Gu Z, Black Phosphorus Hydrogel Scaffolds Enhance Bone Regeneration Via a Sustained Supply of Calcium-Free Phosphorus. ACS Appl. Mater. Interfaces 2019, 11 (3), 2908–2916. [PubMed: 30596421]

(54). Wang Z; Zhao J; Tang W; Hu L; Chen X; Su Y; Zou C; Wang J; Lu WW; Zhen W; Zhang R; Yang D; Peng S, Multifunctional Nanoengineered Hydrogels Consisting of Black Phosphorus Nanosheets Upregulate Bone Formation. Small 2019, 15 (41), e1901560. [PubMed: 31423735]

(55). Dang PN; Dwivedi N; Yu X; Phillips L; Bowerman C; Murphy WL; Alsberg E, Guiding Chondrogenesis and Osteogenesis with Mineral-Coated Hydroxyapatite and Bmp-2 Incorporated within High-Density Hmsc Aggregates for Bone Regeneration. ACS Biomater. Sci. Eng 2016, 2 (1), 30–42. [PubMed: 33418642]

(56). Dang PN; Dwivedi N; Phillips LM; Yu X; Herberg S; Bowerman C; Solorio LD; Murphy WL; Alsberg E, Controlled Dual Growth Factor Delivery from Microparticles Incorporated within

Human Bone Marrow-Derived Mesenchymal Stem Cell Aggregates for Enhanced Bone Tissue Engineering Via Endochondral Ossification. Stem Cells Transl. Med 2016, 5 (2), 206–217. [PubMed: 26702127]

(57). Li X; Xu L; Nie H; Lei L, Dexamethasone-Loaded B-Cyclodextrin for Osteogenic Induction of Mesenchymal Stem/Progenitor Cells and Bone Regeneration. J. Biomed. Mater. Res. A 2021, 109 (7), 1125–1135. [PubMed: 32981208]

(58). Zhou X; Feng W; Qiu K; Chen L; Wang W; Nie W; Mo X; He C, Bmp-2 Derived Peptide and Dexamethasone Incorporated Mesoporous Silica Nanoparticles for Enhanced Osteogenic Differentiation of Bone Mesenchymal Stem Cells. ACS Appl. Mater. Interfaces 2015, 7 (29), 15777–15789. [PubMed: 26133753]

(59). Liu X; George MN; Li L; Gamble D; Miller II AL; Gaihre B; Waletzki BE; Lu L, Injectable Electrical Conductive and Phosphate Releasing Gel with Two-Dimensional Black Phosphorus and Carbon Nanotubes for Bone Tissue Engineering. ACS Biomater. Sci. Eng 2020, 6 (8), 4653–4665. [PubMed: 33455193]

(60). Wang C; Ye X; Zhao Y; Bai L; He Z; Tong Q; Xie X; Zhu H; Cai D; Zhou Y; Lu B; Wei Y; Mei L; Xie D; Wang M, Cryogenic 3d Printing of Porous Scaffolds for in Situ Delivery of 2d Black Phosphorus Nanosheets, Doxorubicin Hydrochloride and Osteogenic Peptide for Treating Tumor Resection-Induced Bone Defects. Biofabrication 2020, 12 (3), 035004. [PubMed: 31952065]

(61). Gao C; Feng P; Peng S; Shuai C, Carbon Nanotube, Graphene and Boron Nitride Nanotube Reinforced Bioactive Ceramics for Bone Repair. Acta Biomater 2017, 61, 1–20. [PubMed: 28501710]

(62). Liu X; Miller AL; Park S; George M; Waletzki BE; Xu H; Terzic A; Lu L, Two-Dimensional Black Phosphorus and Graphene Oxide Nanosheets Synergistically Enhance Cell Proliferation and Osteogenesis on 3d-Printed Scaffolds. ACS Appl. Mater. Interfaces 2019, 11 (26), 23558–23572. [PubMed: 31199116]

(63). Wang H; Yang X; Shao W; Chen S; Xie J; Zhang X; Wang J; Xie Y, Ultrathin Black Phosphorus Nanosheets for Efficient Singlet Oxygen Generation. J. Am. Chem. Soc 2015, 137 (35), 11376–11382. [PubMed: 26284535]

(64). Chiu R; Ma T; Smith RL; Goodman SB, Polymethylmethacrylate Particles Inhibit Osteoblastic Differentiation of Mc3t3-E1 Osteoprogenitor Cells. J. Orthop. Res 2008, 26 (7), 932–936. [PubMed: 18302244]

(65). Hassan MN; Yassin MA; Suliman S; Lie SA; Gjengedal H; Mustafa K, The Bone Regeneration Capacity of 3d-Printed Templates in Calvarial Defect Models: A Systematic Review and Meta-Analysis. Acta Biomater 2019, 91, 1–23. [PubMed: 30980937]

(66). Kim JA; Yun H.-s.; Choi Y-A; Kim J-E; Choi S-Y; Kwon T-G; Kim YK; Kwon T-Y; Bae MA; Kim NJ, Magnesium Phosphate Ceramics Incorporating a Novel Indene Compound Promote Osteoblast Differentiation in Vitro and Bone Regeneration in Vivo. Biomaterials 2018, 157, 51–61. [PubMed: 29245051]

(67). Yang B; Yin J; Chen Y; Pan S; Yao H; Gao Y; Shi J, 2d-Black-Phosphorus-Reinforced 3d-Printed Scaffolds: A Stepwise Countermeasure for Osteosarcoma. Adv. Mater 2018, 30 (10), 1705611.

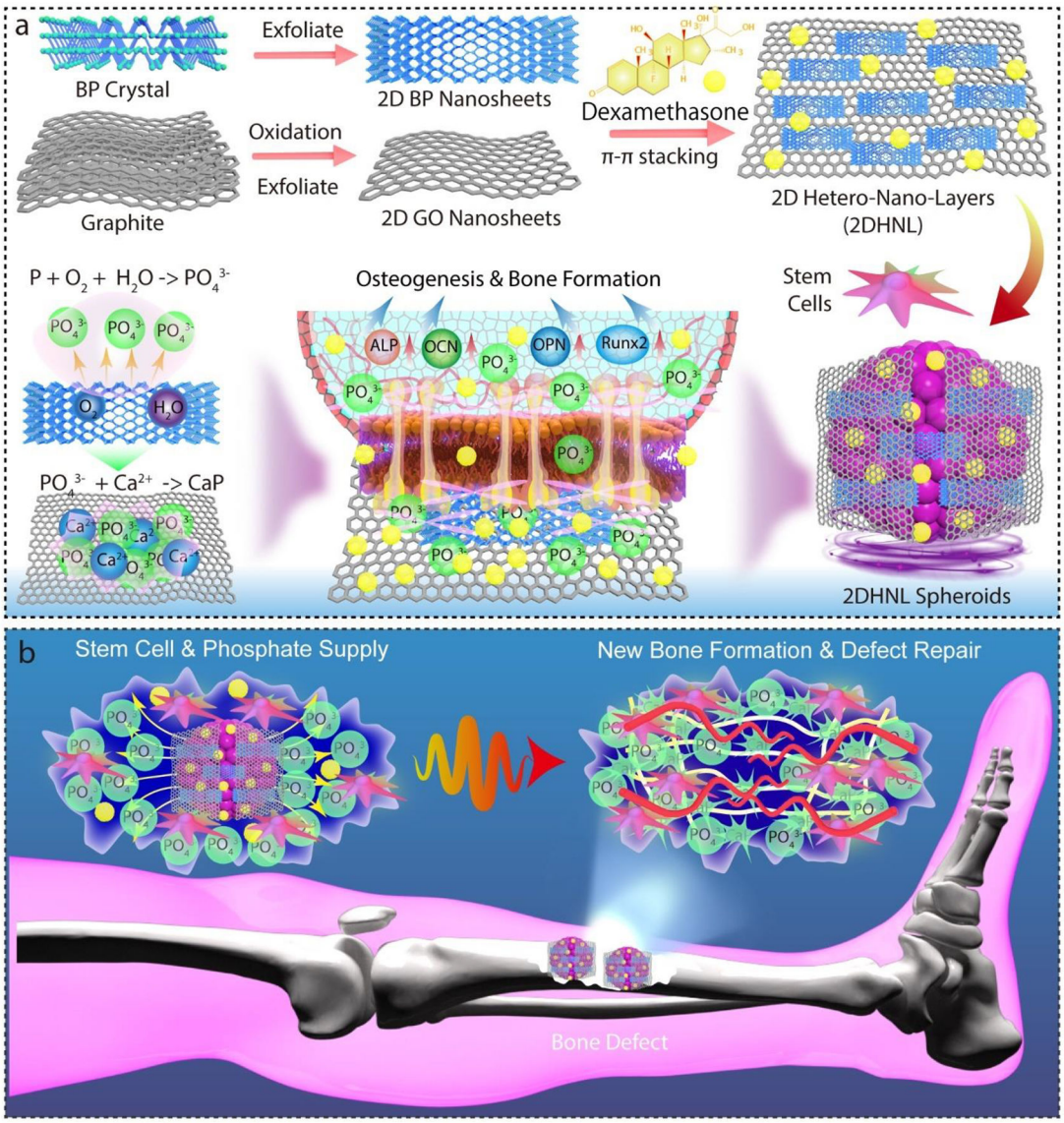

Fig. 1.

Schematic demonstration of the injectable functionalized stem cell organoids for bone regeneration. a) The fabrication of 2D black phosphorus (BP) and graphene oxide (GO) nanosheets by exfoliation and construction of stem cell spheroids functionalized with BP and GO hetero-nano-layers (HNL). The sustained release of phosphate ions by BP oxidation and enhanced biomineralization deposition due to the large surface area of GO stimulated the osteogenesis of stem cells through the elevated expression of osteogenic proteins, including alkaline phosphatase (ALP), osteopontin (OPN), osteocalcin (OCN), and runt-related transcription factor 2 (Runx2). b) An operative scheme of inspirational stem cell/osteogenic factor co-delivery strategy using spheroids and two-dimensional hetero-nano-layers for enhanced bone regeneration.

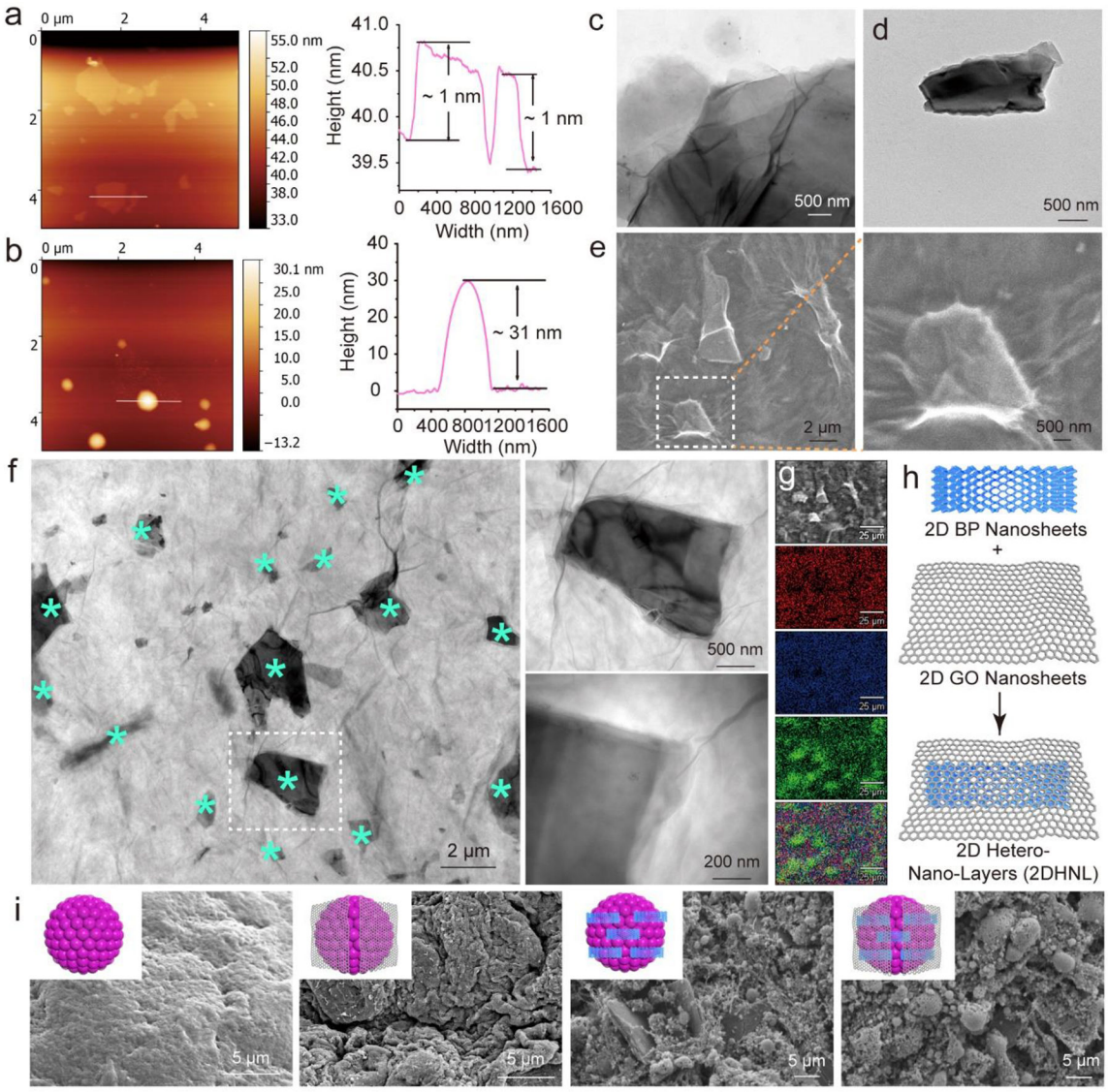

Fig. 2.

Material characterizations. AFM imaging and height profile of a) 2D GO nanosheets and b) 2D BP nanosheets. TEM images of c) GO and d) BP nanosheets. Detailed e) SEM images and f) TEM images of BP nanosheets (marked with *) wrapped with GO nanosheets. g) Element mapping of carbon (red), oxygen (blue), and phosphorous (green) of GO@BP mixtures. h) Schematic demonstration of wrapping BP with GO nanosheets to create 2DHNL. i) SEM image of pure stem cell spheroids and functionalized spheroids that incorporated with GO, BP, and GO@BP nanosheets.

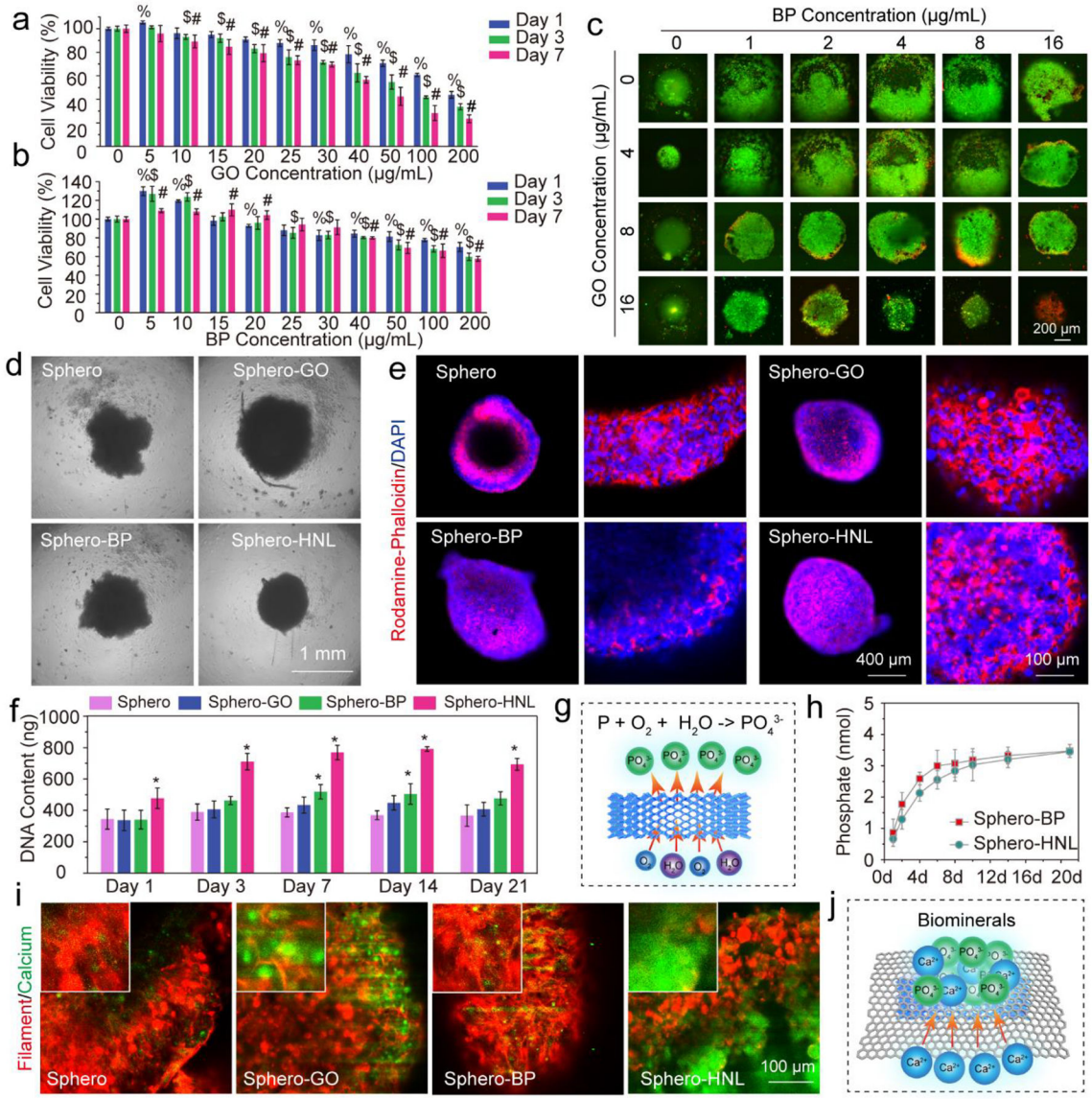

Fig. 3.

Spheroids formation and characterization. *In vitro* stem cell cytotoxicity of a) GO nanosheets and b) BP nanosheets at various concentrations. c) Stem cell spheroids live/dead staining at 3 days after the incorporation of various concentrations of GO and BP nanosheets. d) Photograph of MSC spheroids (Sphero) and spheroids incorporated with GO nanosheets (Sphero-GO), BP nanosheets (Sphero-BP), and GO@BP HNL (Sphero-HNL) at day 1. e) Immunofluorescent images of whole MSC spheroids and their enlarged edge views at day 7 (red: rhodamine-phalloidin; blue: DAPI). f) DNA contents of the four groups of spheroids. g) Phosphate ion release by the oxidation of BP nanosheets. h) Phosphate ion release kinetics from spheroids incorporated with BP and GO@BP HNL. i) Calcium deposition in spheroids as visualized by calcein stain (green) and F-actin staining (red) after 14 days of culture. j) Potential mechanism of biomineral deposition taking advantage of

large surface areas of 2D materials. (%, $, #: $p < 0.05$ to control group (0 μg/mL); *: $p < 0.05$ to Sphero group).

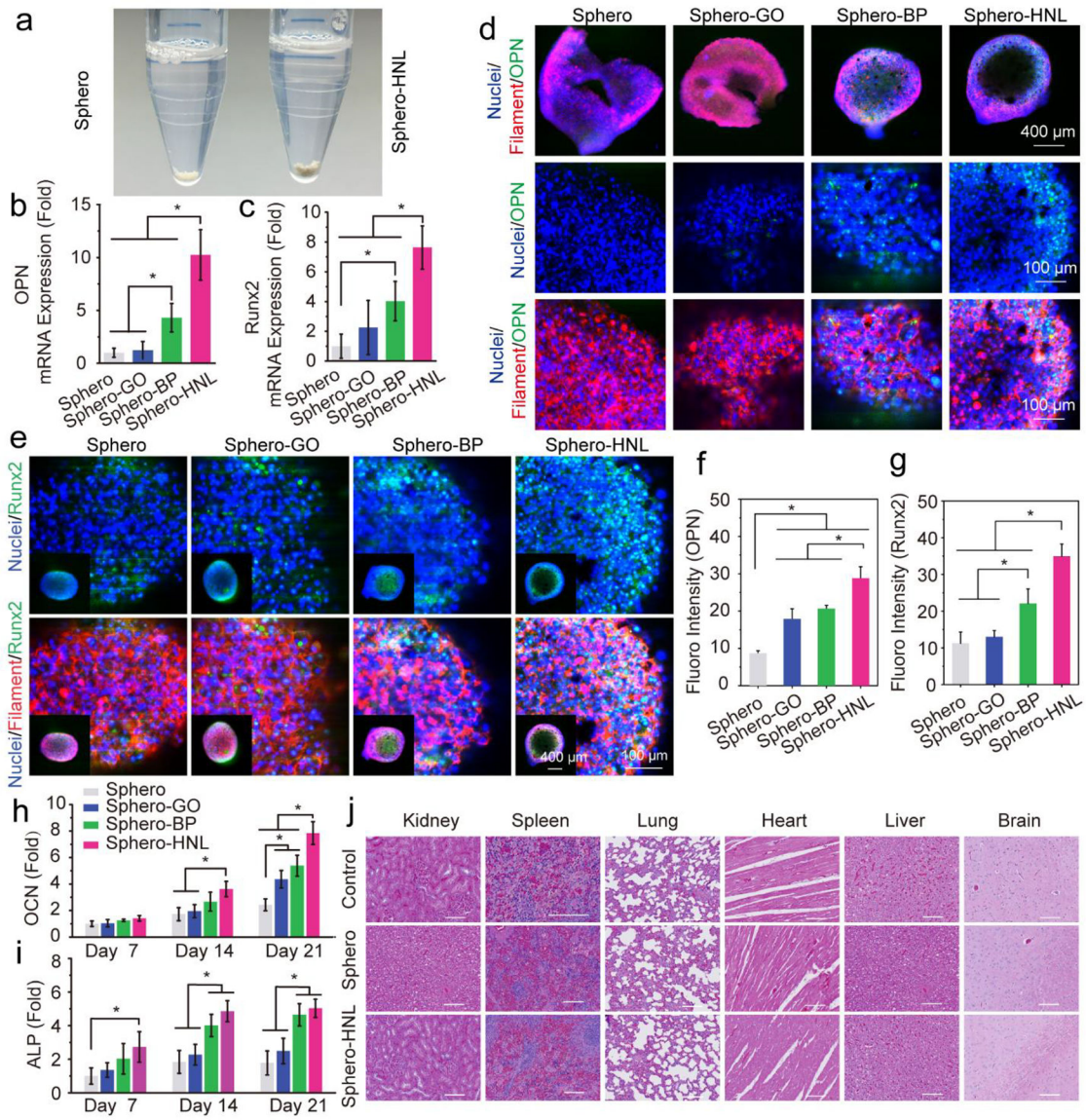

Fig. 4.

Osteogenesis of stem cell spheroids. a) Photographs of the Sphero and Sphero-GO@BP. The mRNA expressions of osteogenic markers b) OPN and c) Runx2 in stem cell spheroids after 14 days of culture. d) Immunofluorescent imaging of osteogenic OPN protein (green), F-actin (red), and nuclei (blue) in stem cell spheroids. e) Immunofluorescent imaging of osteogenic Runx2 protein (green), F-actin (red), and nuclei (blue) in stem cell spheroids. Quantified fluorescence intensity for f) OPN and g) Runx2 markers in spheroids. h) Relative OCN content and i) ALP activity of stem cell spheroids. j) Histological staining of the major organs of rats after 8 weeks of implantation with spheroids (scale bar: 200 μm). (*: $p < 0.05$).

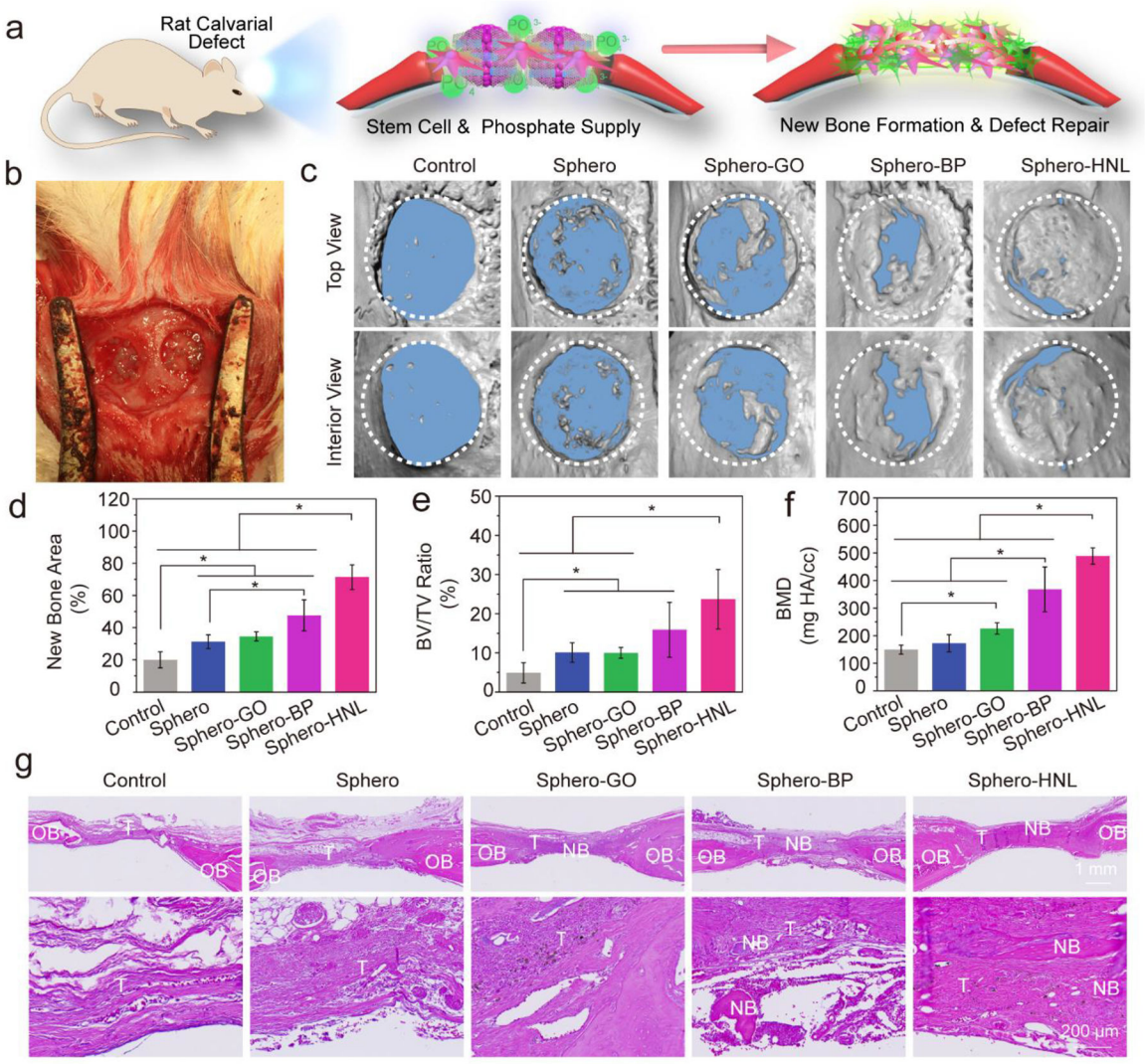

Fig. 5.

In vivo bone formation in rat calvarial defects. a) Schematic demonstration of bone formation in defects treated with stem cell spheroids and b) photograph of *in vivo* implantation of the spheroids. c) Micro-CT reconstruction of the rat cranial defect only (Control) or defects with stem cell spheroids after 8 weeks of implantation. Quantitative analysis of d) bone area, e) bone volume/tissue volume ratio, and f) bone mineral density. g) H & E staining of tissue samples from rat cranial defects without (Control) or with stem cell spheroids. NB: New Bone; OB: Original Bone; T: Tissue. (*: $p < 0.05$).

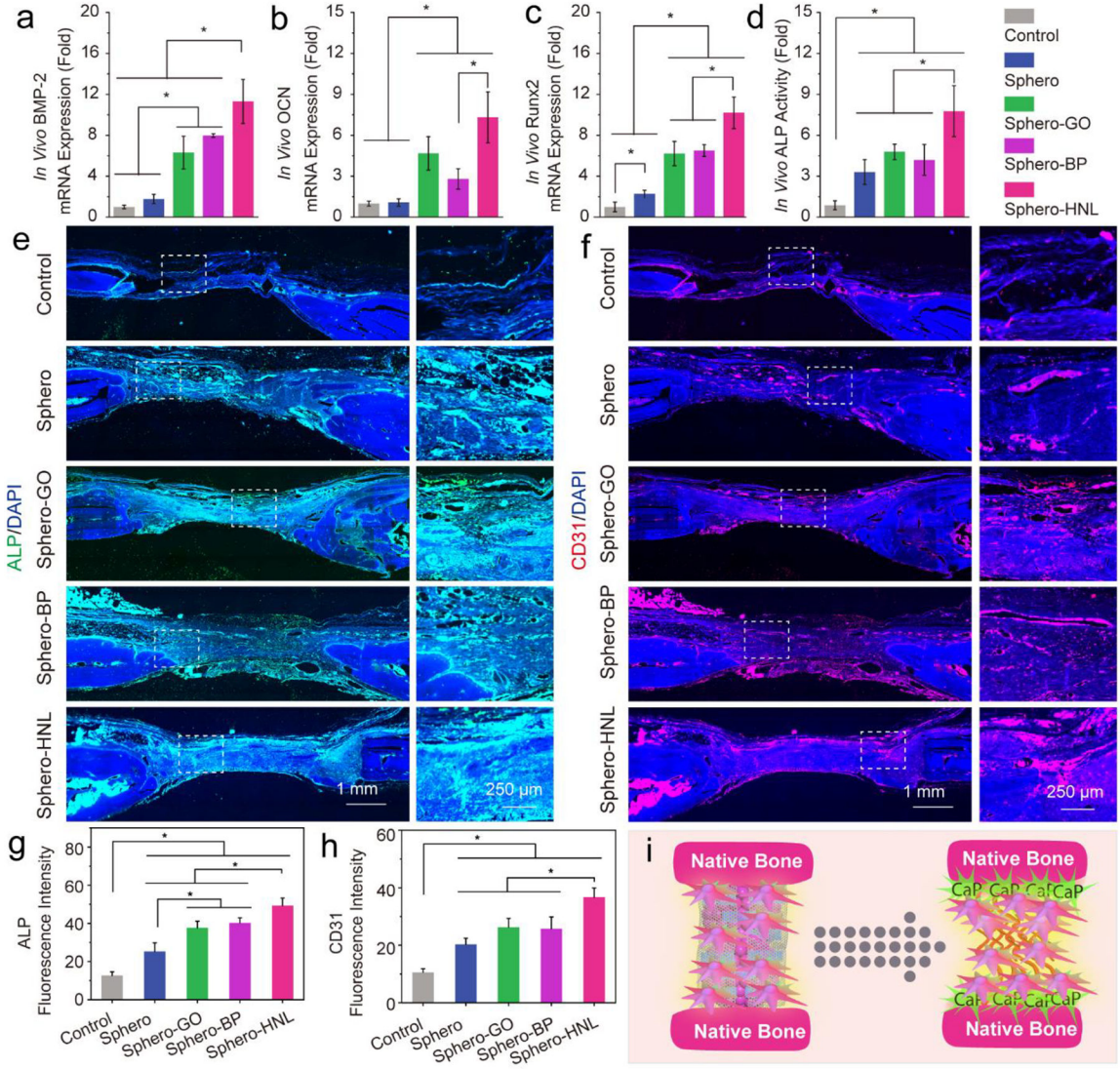

Fig. 6.

In vivo neovascularization and osteogenesis in rat calvarial defects. *In vivo* mRNA expression of a) BMP-2, b) OCN, and c) Runx2 and d) *in vivo* ALP activity after 8 weeks. Immunohistochemistry staining of e) ALP (green) with nuclei (blue) and f) CD31 (red) with nuclei (blue) in untreated rat cranial defects (Control) or defected implanted with various stem cell spheroids after 8 weeks. Quantified fluorescence intensity of g) ALP and h) CD31 marker. i) Schematic demonstration of *in vivo* osteogenesis and neovascular formation in the defect area.

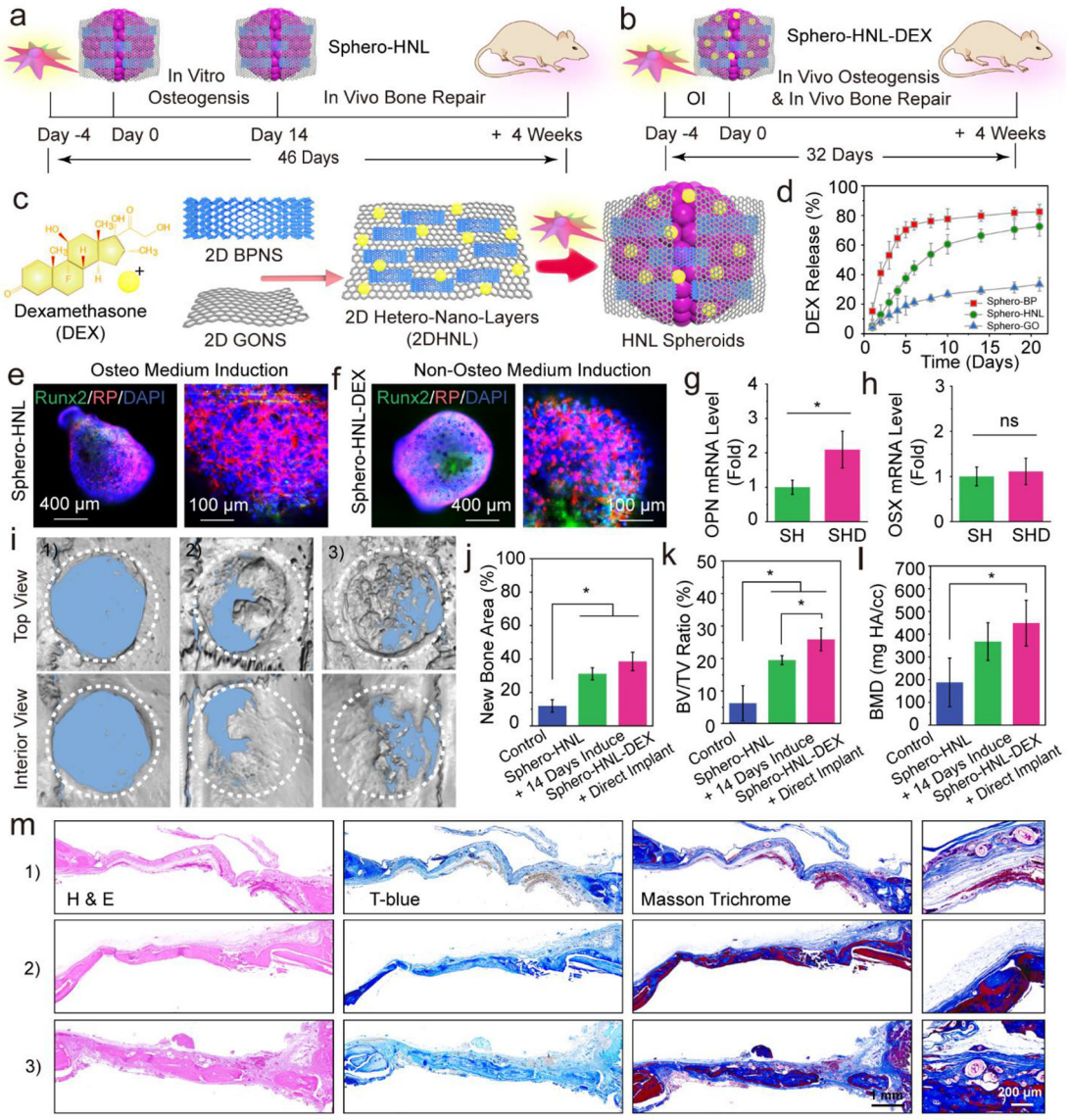

Fig. 7.

An all-in-one system for *in vivo* stem cell and osteogenic factor co-delivery enabling bone formation during a shorted overall treatment time. a) Current strategy using stem cell spheroids encapsulating GO@BP hetero-nano-layers (Sphero-HNL) for bone formation. b) Proposed strategy using Sphero-HNL loaded with DEX for *in vivo* osteogenesis and bone formation. c) Fabrication of DEX-loaded GO@BP hetero-nano-layers and stem cell spheroids. d) The *in vitro* DEX release kinetics during a 21-day period. Immunofluorescence staining of Runx2 osteogenic marker in e) Sphero-HNL after induction using the osteogenic medium for 14 days and f) Sphero-HNL-DEX after incubation using the non-osteogenic medium for 14 days. The mRNA expressions of osteogenic markers g) OPN and h) OSX in stem cell spheroids (SH: Sphero-HNL in osteogenic medium; SHD: Sphero-HNL-DEX in non-osteogenic medium). i) Micro-CT reconstruction of the untreated rat cranial defect and defects after 4 weeks of implantation with Sphero-HNL induced by osteogenic medium

for 14 days and Sphero-HNL-DEX without *in vitro* induction. Quantitative analysis of j) bone area, k) bone volume/tissue volume ratio, and l) bone mineral density. m) H & E staining, Toluidine blue staining, and Masson's trichrome histochemical staining of tissue samples from rat cranial defects: 1) empty control, 2) defects implanted with Sphero-HNL induced by osteogenic medium for 14 days, and 3) defects directly implanted with Sphero-HNL-DEX without *in vitro* induction. NB: New Bone; OB: Original Bone; T: Tissue. (*: $p < 0.05$; ns: not significant).

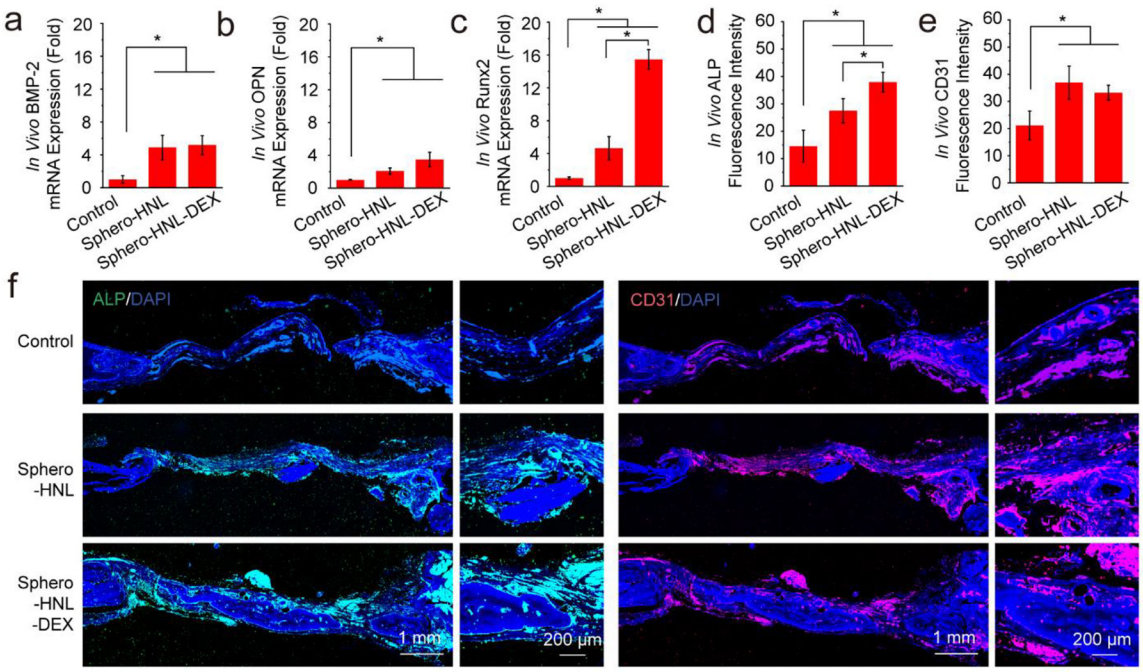

Fig. 8.

In vivo osteogenesis and neovascularization in rat calvarial defects. *In vivo* mRNA expression of a) BMP-2, b) OCN, and c) Runx2 after 4 weeks. Quantified fluorescence intensity for d) ALP and e) CD31 marker. f) Immunohistochemistry staining of CD31 (red) with nuclei (blue) and ALP (green) with nuclei (blue).